A preliminary experimental study on the airfoil self-noise of an oscillating NACA 65-410

B. Zang*, Yannick D. Mayer† and Mahdi Azarpeyvand‡

Faculty of Engineering, University of Bristol, United Kingdom

The present study experimentally investigates a NACA 65-410 cambered airfoil under oscillating motions at moderate Reynolds number. Two oscillation frequencies were tested, which corresponded to a reduced frequency factor, below and above that representative of dynamic stall (i.e. $k_r > 0.05$). Effects of the oscillation frequency, oscillation amplitude as well as the mean oscillation angle of attack on the far-field noise and near-field surface pressure fluctuations were examined. In general, an increase in both the oscillation amplitude and frequency results directly an increase in the far-field noise of an oscillating airfoil, at relatively high mean angles of attack. From the near-field pressure measurements, the surface pressure fluctuations are seen to be either comparable or consistently higher for the oscillating airfoil, as compared to its static counterpart, consistent with previous findings. Moreover, a detailed coherence map along the chordwise direction reveals that while the coherence increases and spreads towards the leading-edge at low mean angles of attack, it reduces when the flow begins to separate from the airfoil. Short-time Fourier transform analyses of the oscillating airfoil show that for the separated flow conditions, the energy contents are concentrated in the low frequency regions throughout a full oscillation cycle.

Nomenclature

α	angle of attack [°]
α_{avg}	angle of attack [°]
Λ	amplitude of the airfoil oscillation [°]
c	aerofoil chord length [mm]
f	frequency [Hz]
k_r	reduced frequency factor [-]
ϕ_{pp}	Fourier-transformed spectra of the surface pressure fluctuations [-]
γ^2	coherence between measured dynamic pressure field [-]
Re_c	Reynolds number based on chord length [-]
U_∞	free stream velocity [m/s]
Ω	temporal frequency of the airfoil oscillation [-]
x	coordinate chordwise direction [-]
y	coordinate vertical direction [-]
z	coordinate along the spanwise direction [-]
PSD	power spectral density [dB/Hz]
$STFT$	Short-time Fourier Transform analyses [-]

*Research Associate, Department of Aerospace Engineering, University of Bristol.
†Ph.D. Researcher, Department of Aerospace Engineering, University of Bristol.
‡Professor of Aerodynamics and Aeroacoustics, Department of Mechanical Engineering, University of Bristol.

I. Introduction

Aeroacoustic noise from a dynamically oscillating airfoil has been of particular interest to engineering applications since the majority of blades (i.e. helicopters and turbines) were subjected to dynamically-varying loads under normal operating conditions.[1] For instance, Smith *et al.*[2] analyzed the amplitude modulation phenomenon from the turbine blades and concluded that dynamically changing conditions such as wind shear, wake periodicity and large scale turbulence structure, could play an significant role in the noise characteristics of a rotating turbine blade and produce a phenomenon known as 'other amplitude modulations'. Similar conclusions were also reached by Oerlemans,[3] Choudhry *et al.*[4] and Laratro *et al.*[5] from their experiments on the operating wind turbines with non-uniform inflow conditions. While most experiments conducted in the laboratory environment remain static, it is necessary to design and perform experiments of airfoils with dynamic oscillations in order to better understand the complexity of the problem, and furthermore help improve the accuracy of prediction and numerical models. Nagarajan *et al.*[6] examined numerically the flow past an oscillating NACA 0012 airfoil using Large-eddy and Unsteady RANS (URANS)simulations at moderate Reynolds number and reported an increase in the broadband noise, as compared to its static counterpart. More recently, Zajamsek *et al.*[7] conducted a set of experiments to study the aeroacoustic noise from rotating NACA 0012 airfoils at moderate Reynolds number of Re = 240,000 and concluded that the trailing-edge noise from the oscillating airfoil contributed as the primary noise source at the outer section of the rotating airfoils. This was later confirmed by the experiments performed by Zhou *et al.*[8] Furthermore, they reported that the airfoil oscillation lead to an increase in the broadband noise with a decrease in the tonal peaks. More recently, Mayer *et al.*[9] recently investigated the near-field characteristics of an dynamically stalled NACA 0012 airfoil at moderate Reynolds number, and found that the time-averaged surface pressure fluctuations constantly exceeded those with a statically stalled airfoil.

As seen from literature, numerical and experimental studies on oscillating airfoils are much limited compared to the static counterparts, and in addition, majority of the studies have focused on the simple flat-plate shape or symmetric airfoils. Siegel *et al.*[10] carried out a set of experiments to understand the dynamic stall of a NACA 64-618 airfoil and the largest noise increase was discovered to be at low frequencies at approximately 200Hz. Indeed, from the practical engineering perspective, rotor and/or turbine blade profiles are often cambered, and thus a cambered NACA series is considered as a preferred 'starting point' for the engineering design process. Therefore, it is both interesting and timely to conduct experiments to investigate the aerodynamic and aeroacoustic behaviors of an oscillating cambered airfoil. The present experiments consist of a preliminary study on the far-field airfoil self-noise and the near-field aerodynamic characteristics of a highly instrumented NACA 65-410 airfoil under sinusoidal oscillations, which aims to contribute to the database of a cambered NACA 65-410 airfoil under dynamic motion as well as to shed some new light on the near-field dynamics and far-field noise of an oscillating airfoil.

II. Experimental setup

The present experiments have been carried out in the closed-circuit open-jet aeroacoustic wind tunnel at University of Bristol. The anechoic chamber has a anechoic frequency of 160Hz[11] and is temperature controlled to maintain a relatively constant experimental condition throughout the period of experiments. The open-jet nozzle is 0.775m in height and 0.5m in width with a maximum attainable free stream velocity of $U_\infty = 40\text{ms}^{-1}$, which is designed to allow measurements of an airfoil at low to moderate Reynolds numbers. As shown in Fig. 1, the airfoil is mounted inside a test section with both the top and bottom being fitted with Kevlar clothes, uniformly tensioned throughout the span. The Kevlar wall allows acoustic waves to transimit to far-field without expanding the flow,[12] as such to minimize the corrections on the effective angle of attack which is essential for experiments into high angles of attack. The characteristics and performance of the Kevlar-walled test section have been recently reported by Mayer *et al.*[13]

A. Servo Motor and the Oscillation Motion

The unsteady airfoil motion was controlled using a Nidec 095E3E-FM servo motor driven by a M700 Nidec servo drive with a MCi210 application module, and sinusoidal oscillation profiles with varying oscillation amplitude and frequencies were specified during the experiments. McCroskey[14] determined that airfoils became dynamically stalled with a reduced frequency factor of $k_r > 0.05$, where the reduced frequency

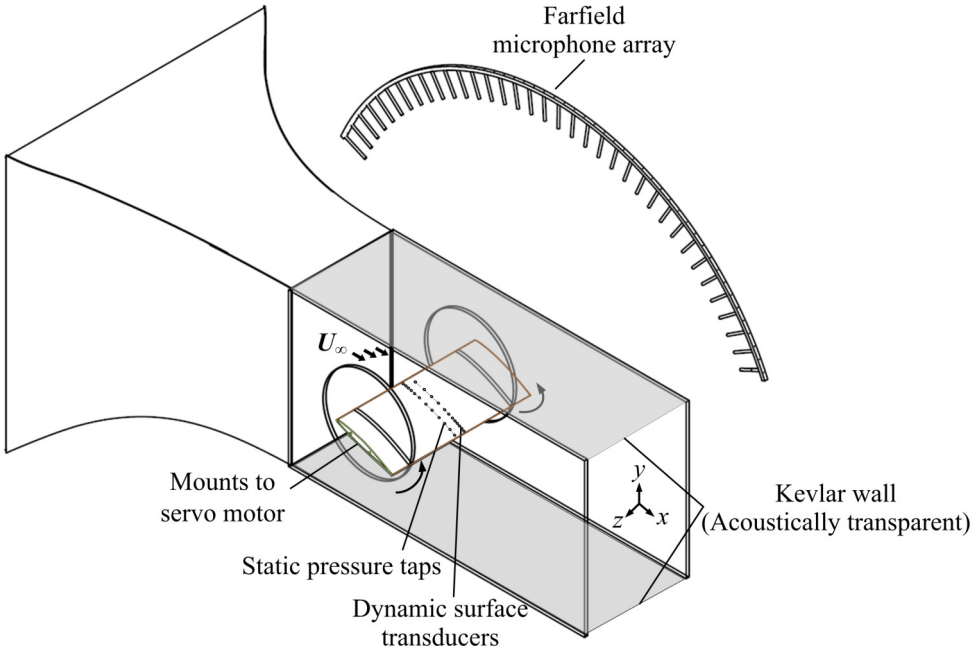

Figure 1: Schematic of the experimental setup on the oscillating NACA 65-410.

factor was defined as:

$$k_r = \frac{c\pi\Omega}{U_\infty} \tag{1}$$

Here, c refers to the chord length, Ω is the oscillating frequency and U_∞ the free stream velocity. To examine the effects of both oscillation frequency and amplitude on the aerodynamic and aeroacoustic characteristics of an oscillating airfoil, two different oscillating frequencies at $\Omega = 0.5$Hz and 1.1Hz, which corresponded to reduced frequency factors of $k_r = 0.023$ and 0.052 and three distinct oscillation amplitudes of $\Lambda = 4°$ 6° and 8° were programmed and executed during experiments. Moreover, in order to study the airfoil oscillation for a range of flow conditions over the airfoil from low (attached) to high (separated and stall) angles of attack, three averaged angles of attack of $\alpha_{avg} = 0°$, 7° and 12° were used as representatives. As such, the airfoil oscillatory motion can be expressed as:

$$\alpha(t) = \alpha_0 + \Lambda(1 - cos(2\pi\Omega t)), \tag{2}$$

where Λ denotes the oscillation amplitude and α_0 is the base (i.e. minimum) angle of attack, so that $\alpha_{avg} = \alpha_0 + \Lambda$. Note that the sinusoidal oscillation was initialized from the minimum angle of attack to provide a smooth rump-up motion.[13] Figure 2 shows the comparison between the theoretical sinusoidal motion and the actual motion registered from the motor at $\Omega = 0.5$Hz and 1.1Hz for oscillation amplitude of $\Lambda = 4°$ and 8°, respectively. As can be observed, the actual motion followed satisfactorily to that of a sinusoidal curve, despite some minor under- and overshoots for both oscillation frequencies. the maximum discrepancy between the theoretical and actual angle of attack remains below 5%, under the present experimental conditions. To facilitate the discussion later, a summary of the different test cases have been listed in Table. 1.

α_{avg} (°)	Ω (Hz)	Λ (°)
0	0.5, 1.1	4, 6
7	0.5, 1.1	4, 6, 8
12	0.5, 1.1	4, 6, 8

Table 1: Summary of the different oscillation frequencies (Ω), oscillation amplitudes (Λ) and averaged angle of attack (α_{avg}), for the present experimental tests.

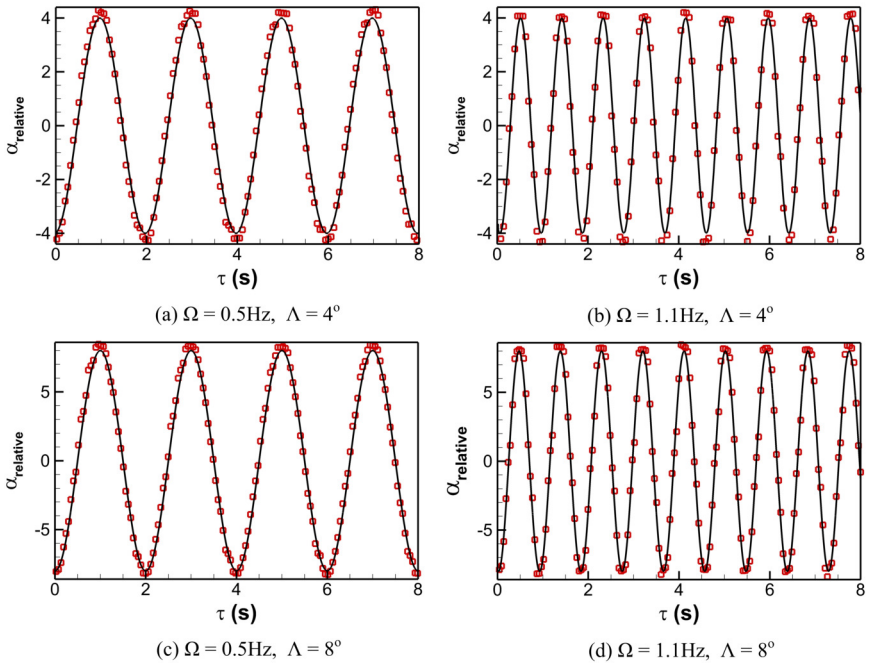

Figure 2: Comparison between the theoretical sinusoidal curve and the actual airfoil motion at (a) Ω = 0.5Hz, Λ = 4°, (b) Ω = 1.1Hz, Λ = 4°, (c) Ω = 0.5Hz, Λ = 8° and (b) Ω = 1.1Hz, Λ = 8°.

B. NACA 65-410 Airfoil and Experiments

A NACA 65-410 airfoil profile, manufactured from Aluminium, was selected as the cambered airfoil as this NACA airfoil has long been recognized as the design 'starting point' for various engineering applications.[15] Measuring with a chord of c = 300mm and a span of 700mm, the airfoil was tripped with a 6mm wide and 0.5mm thick zig-zag turbulator tape at approximately $x/c = 0.1$, on both the pressure and suction sides of the airfoil to allow the development of boundary layer into a fully turbulent state. In order to obtain a comprehensive understanding on the near-field aerodynamic and aeroacoustic characteristics of the oscillating airfoil, the airfoil was equipped with 80 miniature microphones, along both the chordwise and spanwise locations. The dynamic surface pressure transducers were placed in-situ underneath a 0.4mm pinhole, to reduce the sensing area and thus spectral surface pressure attenuation effects.[16] Knowles FG-23629-P16 condenser microphones were used as a direct sensing surface pressure transducers up to x/c = 0.885, whereas Panasonic WM-61A microphones were used as remote sensing pressure transducers until the trailing-edge at $x/c = 0.98$, due to limited space within the hollow airfoil model. All surface pressure transducers were calibrated against a G.R.A.S. 40PL free field microphone, prior to the experiments, which the later was also calibrated with a 42AA Pistophone. As shown in Fig. 1, the far-field noise was collected

through an overhead far-field microphone array consisting of 23 G.R.A.S 40PL microphones. The microphone array, located at about 1.75m above the airfoil model, spans across polar angles of 40° to 150° with a 5° interval, with the 90° microphone aligned directly on top of the airfoil trailing-edge.

The experiments have been performed with a free-stream velocities of 20ms^{-1}, which corresponded to a Reynolds number of Re_c = 422,000 based on the airfoil chord. All near-field surface pressure and far-field noise signals were collected simultaneously by National Instruments PXIe-4499 data acquisition modules at a similar sampling frequency of 2^{15}Hz for 50 oscillation cycles to obtain good statistical convergence on the averaged spectra results. Therefore, the total sampling period for the Ω = 0.5Hz and 1.1Hz oscillation frequencies were 100s and 60s, respectively. Subsequently, to obtain the power spectral density (PSD) of the surface pressure fluctuations, the time-series data were analyzed through Welch's method using a window size of 2^{13} with 50% window overlap and a Hamming window to yield the frequency spectra results. Last but not least, for the Short-Time Fourier Transform analyses (STFT), a total length of five oscillation cycles were analysed. The final frequency resolutions are 4Hz for the frequency spectra and 8Hz for the STFT analyses, with an uncertainty estimated to be approximately 1.5dB based on the window size.[17]

III. Results and Discussion

A. Effects of the oscillation frequency

As a preliminary study to the problem of a cambered oscillating airfoil, it is useful to perform firstly a parametric study on the key parameters such as oscillation frequency (Ω), oscillation amplitude (Λ) as well as the flow conditions over the airfoil (i.e. mean, minimum and maximum angles of attack during the oscillation), to have a better insight into the dynamics of the oscillating airfoil. To begin with, Figs. 3 and 4 show the power spectral density (PSD) of the measured far-field noise of the NACA 65-410 airfoil at different oscillation frequencies of Ω = 0.5Hz and 1.1Hz for mean angles of attack α_{avg} = 0° and 12°, respectively. The PSD has been determined as: $PSD = 10log_{10}(\phi_{pp}/(p_0^2))$, where ϕ_{pp} represents the Fourier-transformed pressure fluctuation spectra and p_0 is the reference pressure of 20μPa. Thus, it should be mentioned here that PSD carries a unit of dB/Hz. The noise spectra for the static airfoil, i.e. airfoil with a fixed angle of attack equivalent to the mean angle of attack for the oscillating airfoil have also been included for reference. As shown in Fig. 3, at a mean angle of attack Λ = 0°, there exist negligible differences on the far-field noise PSD, not only between the two different oscillation frequencies, but also between the static and oscillating airfoils. According to the experiments on an oscillating NACA 0012 airfoil from Mayer *et al.*,[13] the time-averaged quantities of an oscillating airfoil at pre-stalled conditions do not vary notably from its static counterparts. On the other hand, when the mean angle of attack increases to α_{avg} =12°, where the airfoil begins to experience flow separation and stall under the present experimental conditions, the farfield noise PSD clearly illustrate the both the effects of oscillation frequency and the oscillation amplitude. At a smaller amplitude of Λ = 4°, the far-field noise spectra behaves similar to that at lower mean angle of attack. Nevertheless, at the largest oscillation amplitude of Λ = 8°, a noticeable increase can be observed for the oscillation frequency of Ω = 0.5 with more than 2.5dB/Hz across the entire frequency range. Increasing the oscillation further to Ω = 1.1 leads to a further 3 to 4 dB/Hz increase in the far-field noise spectral, which suggests that the airfoil is likely undergoing dynamic stall process. Recall that McCroskey[14] observed dynamic stall of an airfoil when the reduced frequency factor became $k_r > 0.05$, which is fulfilled at Ω = 1.1Hz. This also corresponds well to the observation that the larger oscillation amplitude could lead to more severe lift hysteresis phenomenon which may further contribute to the increased level of far-field noise.[13]

With the knowledge from far-field noise spectra, it will then be interesting to investigate the changes to the near-field surface pressure fluctuations, as the airfoil oscillates. Figure 5 shows the power spectra densities of the surface pressure fluctuations along the chordwise directions from mid-chord location to the trailing-edge, for two oscillation frequencies of Ω = 0.5Hz and 1.1Hz at an oscillation amplitude of Λ = 4°. The static scenario, corresponding to the mean angle of attack has also been included for ease of comparison. Clearly, the magnitude of the PSD is consistently higher for the oscillating airfoils than their static counterparts at α_{avg} = 0°, especially towards the lower frequency range (i.e. f < 1000Hz). For instance, comparing the surface pressure fluctuation PSD of both the oscillating and static airfoil at f=500Hz, the PSD associated with the oscillating airfoils are approximately 76dB/Hz for both oscillation frequencies, whereas is 70dB/Hz for the static case. Therefore, although oscillating about the zero mean angle of attack, the motion elevates the near-field energy frequency contents near the surface of the airfoil.

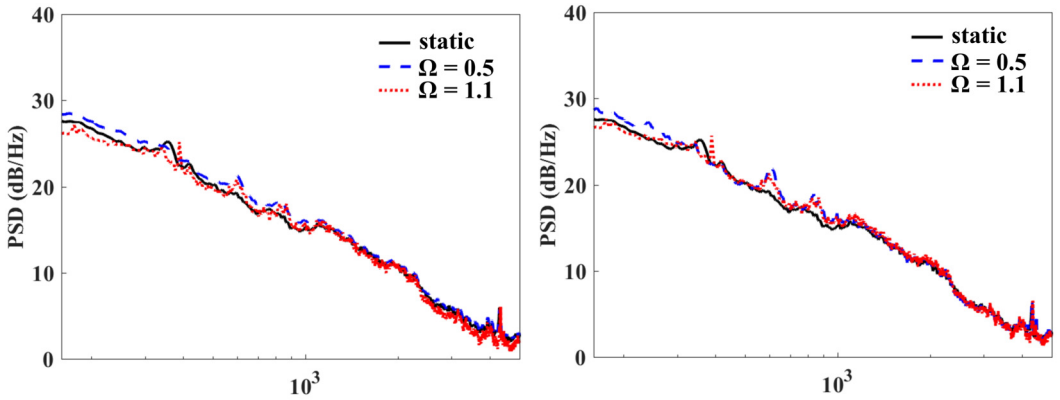

Figure 3: Comparison of the far-field noise spectra between the oscillating airfoils at two different oscillation frequencies of Ω =0.5Hz and 1.1Hz, for oscillation amplitudes of (a) Λ =4° and (b) Λ =6° with mean angle of attack α_{avg}=0°.

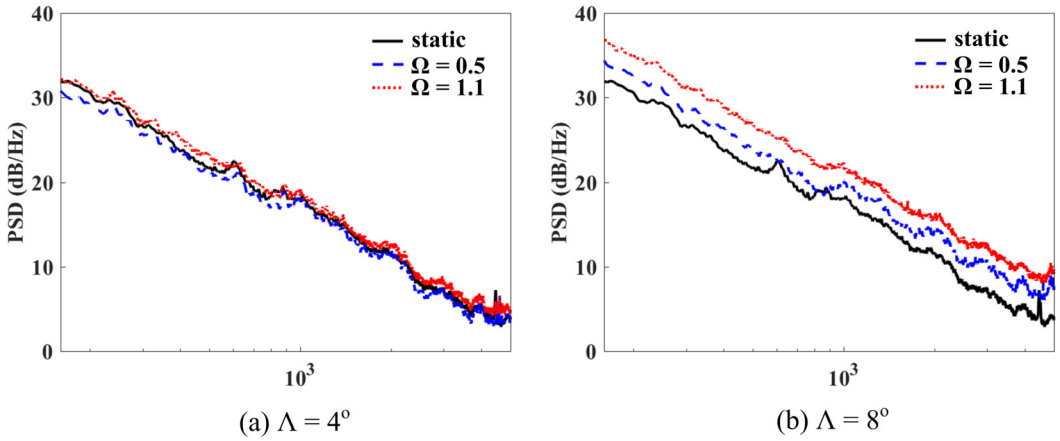

Figure 4: Comparison of the far-field noise spectra between the oscillating airfoils at two different oscillation frequencies of Ω =0.5Hz and 1.1Hz, for oscillation amplitudes of (a) Λ =4° and (b) Λ =8° with mean angle of attack α_{avg}=12°.

At α_{avg}=12°, the surface pressure fluctuation PSD reaffirms that the flow has become separated over the airfoil, as indicated by the monotonically decreasing spectra over the entire frequency range, regardless of the pressure measurement locations. As can be seen from the right hand side of the Fig. 5, the surface pressure fluctuation PSD appear to remain at the comparable level between the oscillating and static airfoils, albeit a minor decrease can be seen for the oscillating airfoils at the very low frequencies of $f < 300$Hz, in contrary to the oscillation at lower mean angle of attack.

Figure 6 shows the coherence (γ^2) contour of the near-field surface pressure fluctuations, with the reference microphones at $x/c = 0.885$. Note that the self-coherence of the reference microphone itself has been omitted in the plots. Also, the static test case at equivalent mean angles of attack have been included for ease of comparison. As can be seen from the results that, distinct characteristics can be observed for low mean angle of attack (α_{avg} =0°) and high mean angle of attack (α_{avg} =12°). At lower α_{avg}, the coherence shows a spread towards the leading-edge of the airfoil, within the range of low frequencies of $f < 500$Hz, which is accompanied by an increase in the surface pressure fluatuation PSD at similar low frequency range, seen earlier in Fig. 5. On the other hand, a loss of coherence can be observed at higher α_{avg}, when the flow separates from the airfoil. The exact nature of the changes to the coherence requires more detailed boundary layer velocity measurements at those surface pressure messurement locations, and hence warrants further analyses and investigations.

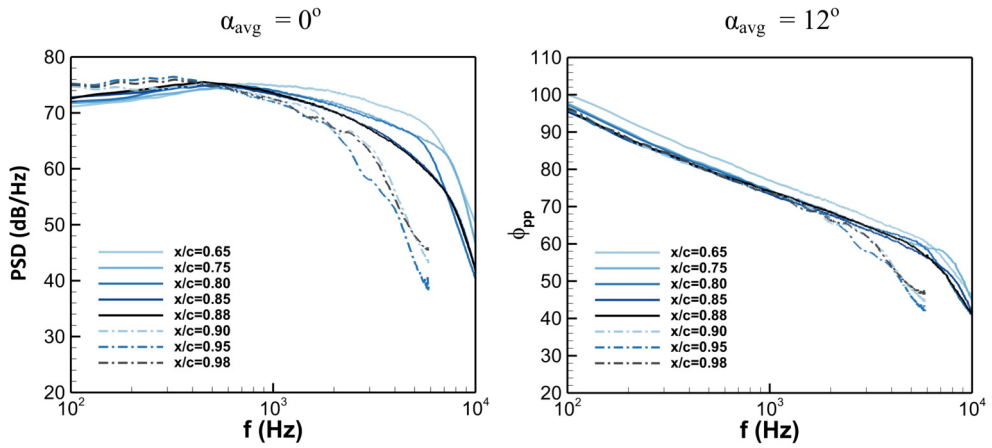

(a) Ω = 0.5Hz

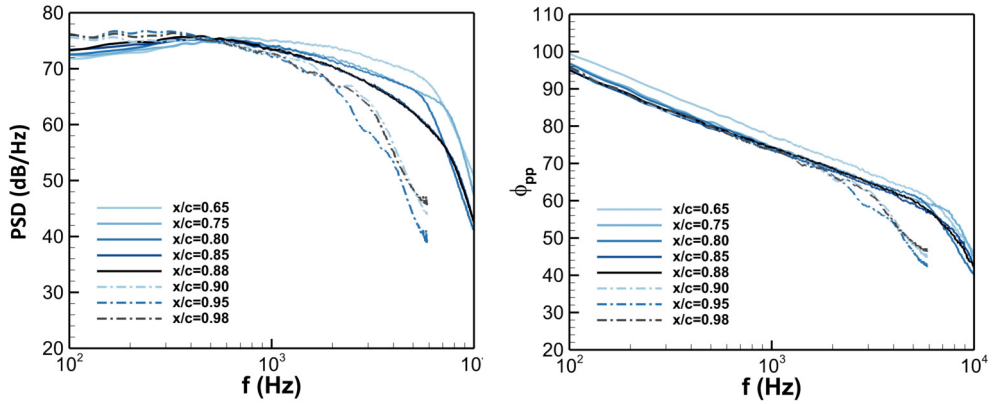

(b) Ω = 1.1Hz

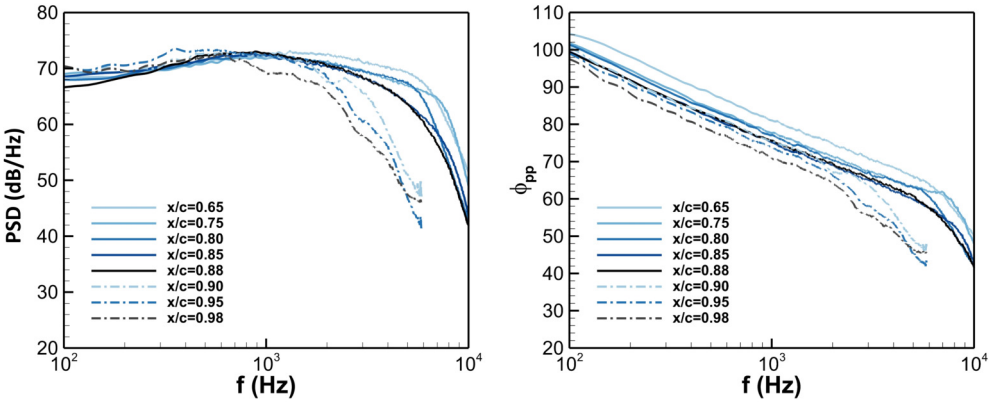

(c) Static

Figure 5: Near-field PSD of the surface pressure fluctuations at various chordwise locations for (a) Ω = 0.5Hz, (b) Ω = 1.1Hz and (c) Static (for comparison) at Λ =4°. Note that α_{avg} denotes the mean angle of attack from the oscillation.

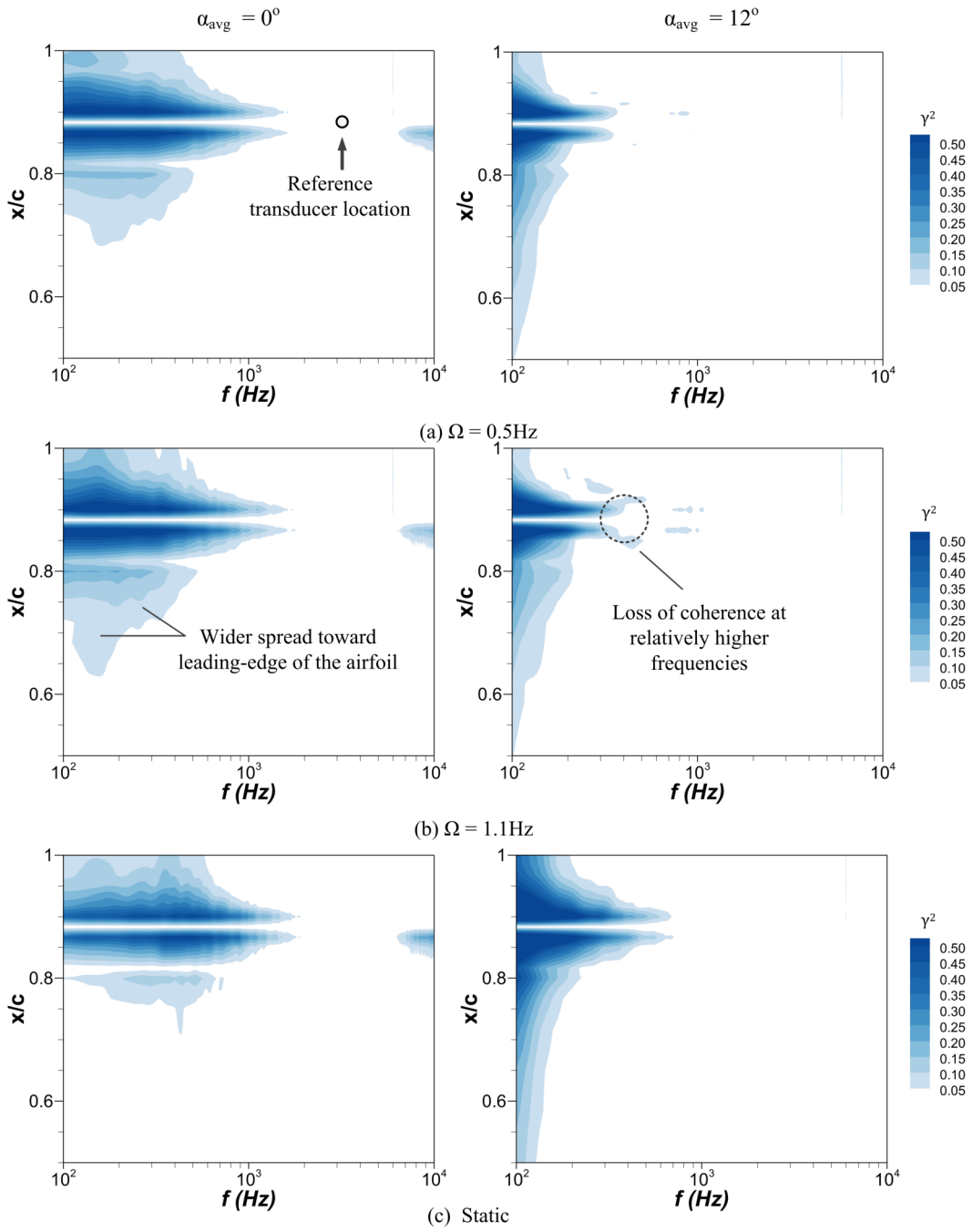

Figure 6: Conherence contour maps of the near-field surface pressure fluctuations at various chordwise locations for (a) $\Omega = 0.5$Hz, (b) $\Omega = 1.1$Hz and (c) Static (for comparison) at $\Lambda = 4°$. Note that α_{avg} denotes the mean angle of attack from the oscillation.

B. Effects of Oscillation Amplitude

With a glimpse of the effects of oscillation amplitude from the far-field noise spectra results above, it is then useful to examine in more details on its effects on both the far-field noise and near-field surface pressure fluctuations. Figure 7 compares the far-field noise spectra at all three oscillation amplitudes of $\Lambda = 4°$, $6°$ and $8°$ at mean angles of attack $\alpha_{avg} = 7°$ and $\alpha_{avg} = 12°$, respectively. Since at $\alpha_{avg} = 0°$, little differences can be observed with the oscillation amplitude, the results are not shown here for brevity. Similar to the observations with varying oscillation frequencies, an increase in the oscillation amplitude leads to higher far-field noise level, when the angle of attack becomes relatively high (i.e. $\alpha_{avg} \approx 7°$ from the present study). Moreover, the increase in the far-field noise is more pronounced when the flow over the airfoil is separated, indicating that a dynamically stalled airfoil is likely to be substantially noisy than a stalled static airfoil.

Figure 8 depict the effects of oscillation amplitude on the near-field surface pressure fluctuations, measured along the chordwise directions from the mid-chord to the trailing-edge of the airfoil, at $\Lambda = 4°$ and $8°$ with a mean angle of attack $\alpha_{avg} = 12°$ and oscillation frequency of $\Omega = 0.5$Hz. Results from both amplitudes appear to be nearly indistinguishable, indicating a consistent dynamic motion of the present experimental setup. However, since the flow has undergone separation, the surface pressure may no longer be very sensitive toward the oscillation amplitudes. To further investigate if the changes to the near-field flow dynamics with different oscillation frequencies is indeed limited, Fig. 9 illustrates the the near-field coherence contour maps at the oscillation frequencies, amplitude and mean angle of attack similar to that of the near-field surface pressure fluctuation PSD in Fig.8. As can be observed from the coherence results, the region of high coherence levels narrows toward the mid-chord location as the the oscillation amplitude increases from $\Lambda = 4°$ to $8°$ in the frequency range of 160Hz $< f$ 200Hz. This could be a hint to the early shedding and separation of the stall vortex from the leading-edge of the airfoil when the airfoil is oscillating with a heightened amplitude.[14]

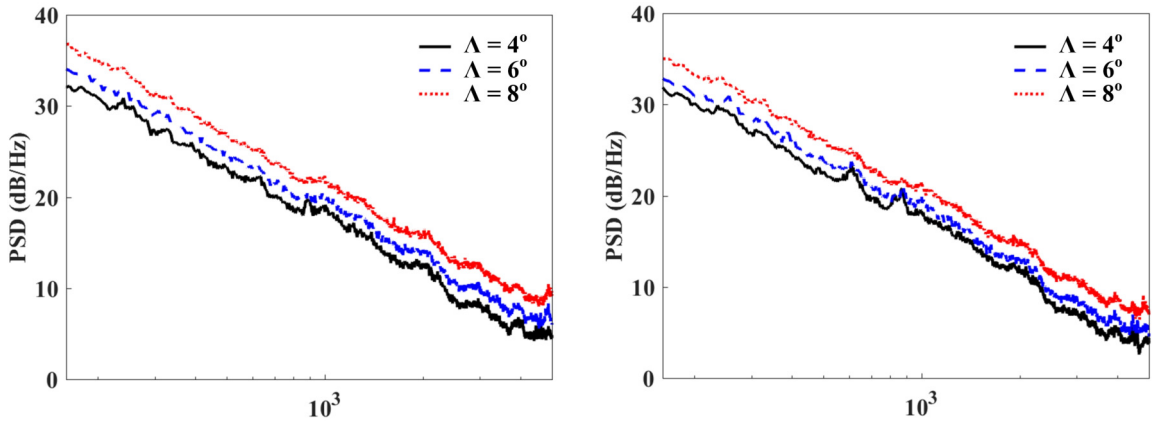

Figure 7: Comparison of the farfield noise spectra between the oscillating airfoils at three different oscillation amplitudes of $\Lambda = 4°$, $6°$ and $8°$, for the mean angles of attack of (a) α_{avg} =7° and (b) α_{avg} =12° with oscillation frequency of $\Omega = 1.1$Hz.

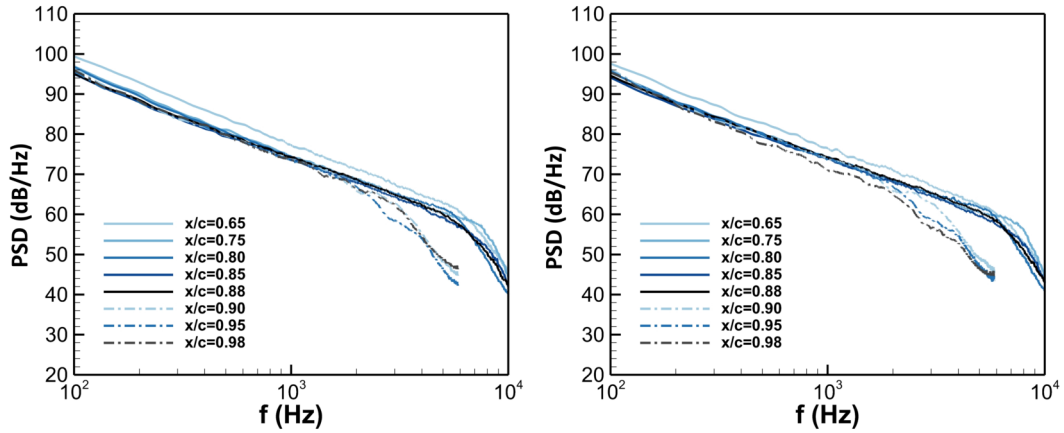

(a) $\Lambda = 4^o$ (b) $\Lambda = 8^o$

Figure 8: Near-field PSD of the surface pressure fluctuations at various chordwise locations for (a) $\Lambda = 4°$ and (b) $\Lambda = 8°$, at mean angle of attack $\alpha_{avg} = 12°$ and oscillation frequency of $\Omega = 1.1$Hz.

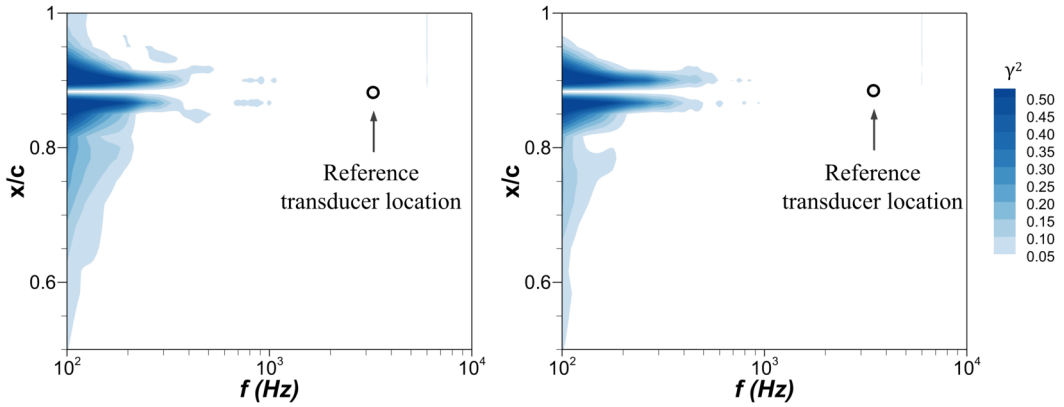

(a) $\Lambda = 4^o$ (b) $\Lambda = 8^o$

Figure 9: Conherence contour maps of the near-field surface pressure fluctuations at various chordwise locations for (a) $\Lambda = 4°$ and (b) $\Lambda = 8°$, at mean angle of attack $\alpha_{avg} = 12°$ and oscillation frequency of $\Omega = 1.1$Hz.

C. Short-Time Fourier Analyses on the Oscillating Airfoil

As highlighted by Mayer *et al.*,[13] Short-Time Fourier Transform (STFT) can be a useful and informative tool when analyzing the airfoil energy frequency contents on the surface pressure fluctuations during the periodic motion. All results here are presented for five oscillation periods. Note that the STFT results are also normalized by $p_0 = 20\mu$Pa. Figure 10 show the STFT analyses results for the two mean angle of attack $\alpha_{avg} = 0^\circ$ and 12° at oscillation frequencies of $\Omega = 0.5$Hz and 1.1Hz and a fixed oscillation amplitude of $\Lambda = 4^\circ$, as representative to the two contrasting flow conditions over the airfoil (i.e. attached and separated). Note that the oscillation cycles are indicated below each contour map for ease of understanding, and in addition, the time scale is multiplied with oscillation frequency Ω (thus, $t\Omega$) to aid the comparison. At $\alpha_{avg} = 0^\circ$ as shown in Figs. 10(a) and (b), the energy distributions are distributed evenly to some large extent across a single oscillation cycle and symmetric about the oscillation peak, except for some short bursts of energy at 'middle' of each oscillation cycle as the airfoil is pitching to the highest angle of attack. At this moment, the flow over the airfoil is experiencing an deceleration followed by an rapid acceleration at the highest angle of attack, probably giving rise an increased level of energy close to the airfoil surface. This also explains that the short bursts of energy intensifies as the oscillation amplitude increases, as shown in Fig. 10(b).

When α_{avg} increases to 12° with the separated flow over the airfoil, the STFT contour maps change drastically. The energy contents are concentrated at low frequency range of $f < 200$Hz during each oscillation cycle. This is in good agreement with the surface pressure coherence contours which showed an increase in the pressure coherence at $f < 200$Hz at high mean angle of attack. Comparing between the two difference oscillation frequencies in 10(c) and (d), it is clear that the energy contents at low frequencies almost span across the entire oscillation cycle, suggesting that the crucial flow events of an oscillating airfoil at stall conditions are associated with low frequencies It is worthwhile to mention that similar observation were made by Seigel *et al.*[10] from their flow visualizations on the oscillating NACA 64-618. The STFT results for two oscillation amplitudes of $\Lambda = 4^\circ$ and 8° for the separated flow conditions (α_{avg} 12°) at oscillation frequency of Ω =1.1Hz is depicted in Fig 11 to complete the analyses on the stalled oscillating airfoils. Indeed, the two STFT contour maps resemble closely to each other with concentrated energy at low frequency regions throughout the oscillation cycle.

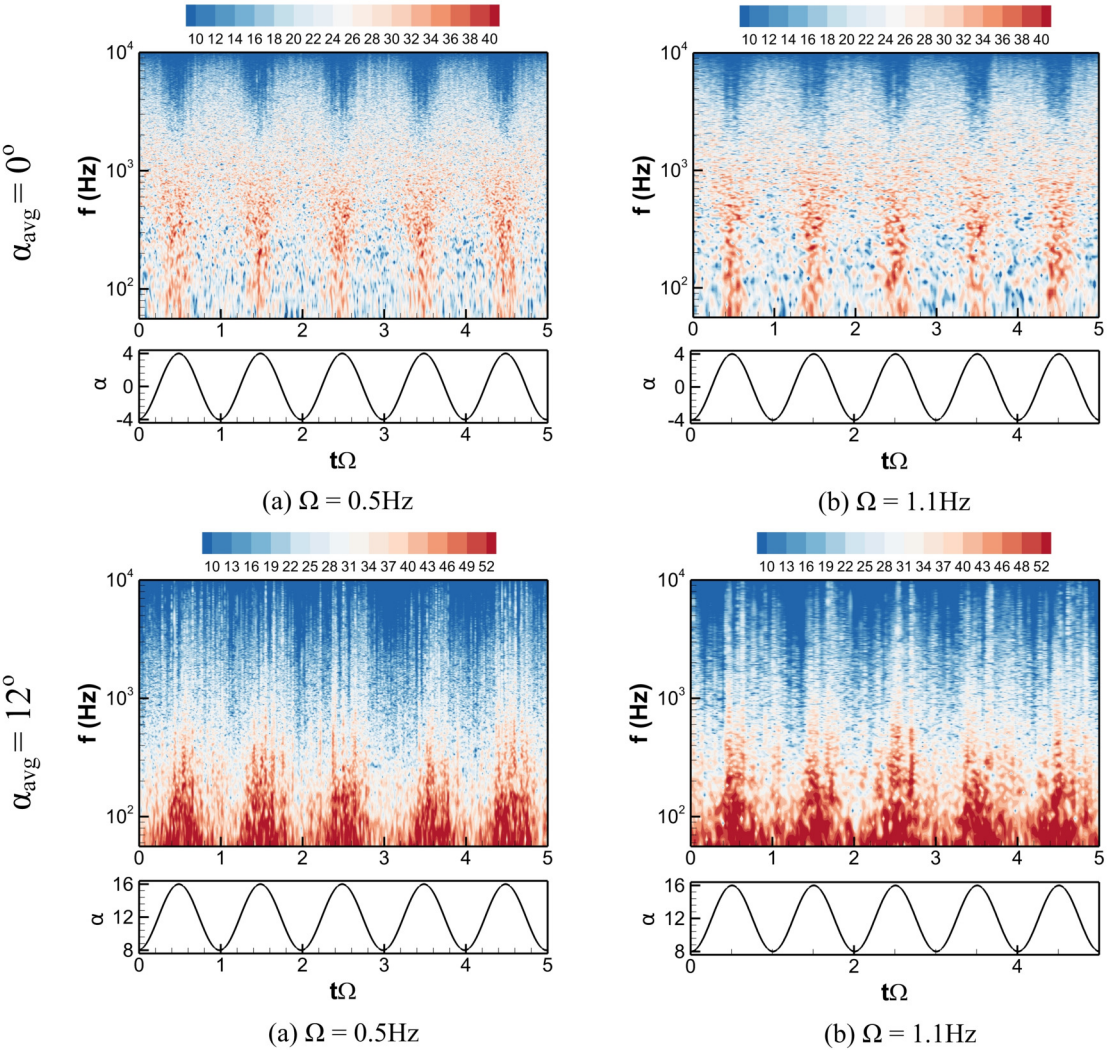

Figure 10: Short-time Fourier transform contour maps for (a) $\Omega = 0.5$Hz, $\Lambda = 4°$ and (b) $\Omega = 1.1$Hz, $\Lambda = 4°$ at α_{avg} =0°, (c) $\Omega = 0.5$Hz, $\Lambda = 4°$ and (d) $\Omega = 1.1$Hz, $\Lambda = 4°$ at α_{avg} =12°.

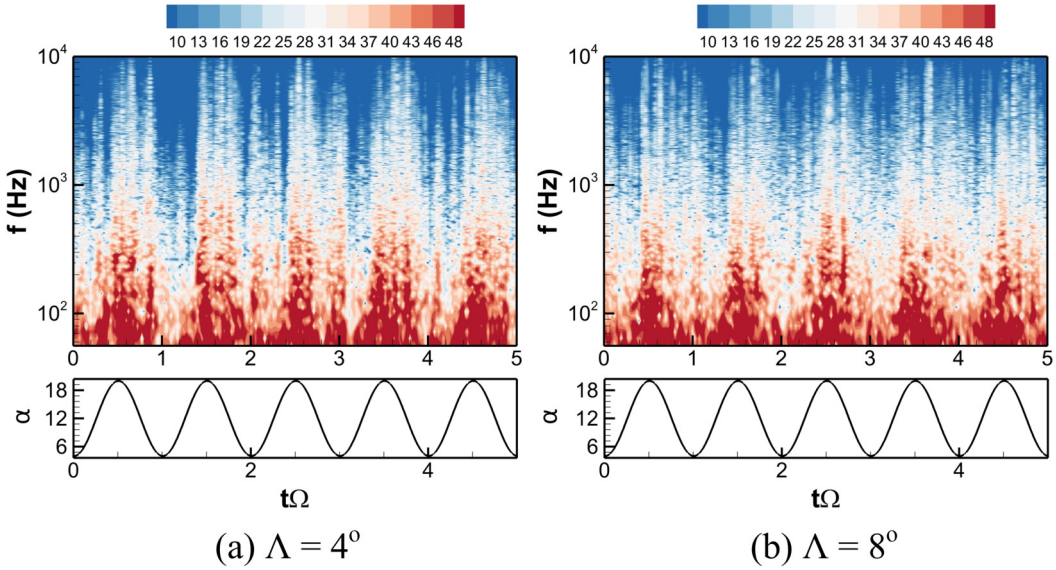

Figure 11: Short-time Fourier transform contour maps for the oscillation amplitudes of (a) $\Lambda = 4°$ and (b) $\Lambda = 8°$ at the mean angle of attack, α_{avg} =12°, and oscillation frequency of Ω =1.1Hz.

IV. Concluding remark

A series of experiments have been conducted to exmamine the near- and far-field aeroacoustic characteristics on an oscillating NACA 65-410 airfoil at moderate Reynolds numbers. By varying the key parameters such as oscillation amplitude, oscillation frequency and mean oscillation angle of attack, their effects on the changes to the far-field noise spectra and near-field surface pressure fluctuations are analysed as a preliminary study to the dynamically oscillating cambered airfoils. From the results, increasing both the oscillation amplitude and frequency will lead to an increase in the far-field noise only at relatively high mean angle of attack. On the other hand, at low mean angle of attack, the changes to the near-field surface pressure of an oscillating airfoil compared to the static airfoil case is more noticeable. An increase in the oscillation amplitude and frequency will produce a greater surface pressure fluctuation PSD level at low frequencies, whereas changes to the near-field surface pressure fluctuations are limited at mean angles of attack where the flow over the airfoil is separated. Last but not least, short-time Fourier transform analyses were performed on the surface pressure fluctuations of the oscillating airfoil over five oscillation cylces to discern the time-dependent flow dynamics. At low mean angle of attack, the energy are approximately evenly distributed except for short bursts of energy as the airfoil approach the highest angle of attack. On the contrary, the energy contents are concentrated at low frequencies when the flow is separated, suggesting that crucial flow dynamics and events occur at low frequencies for the oscillating airfoil at stalled condition.

Acknowledgement

The authors would like to acknowledge the financial support from the EPSRC for the present study via research grant No. EP/R010846/1.

References

[1]Corke, T. C. and Thomas, F. O., "Dynamic stall in pitching airfoils: aerodynamic damping and compressibility effects," *Annual Review of Fluid Mechanics*, Vol. 47, 2015, pp. 479–505.

[2]Smith, M., Bullmore, A., Cand, M., and Davis, R., "Mechanisms of amplitude modulation in wind turbine noise," *Acoustics 2012*, Nantes, France, 2012, pp. 823–828.

[3]Oerlemans, S., "An explanation for enhanced amplitude modulation of wind turbine noise," Technical report nlr-cr-2011-071, National Aerospace Laboratory, Amsterdam, Netherlands, 2011.

[4]Choudhry, A., Mo, J. O., Arjomandi, M., and Kelso, R., "Effects of wake interaction on downstream wind turbines," *Wind Engineering*, Vol. 38, 2014, pp. 535–547.

[5]Larato, A., Arjomandi, M., Kelso, R., and Cazzolato, B., "A discussion of wind turbine interaction and stall contributions to wind farming noise," *Journal of Wind Engineering and Industrial Aerodynamics*, Vol. 127, 2014, pp. 1–10.

[6]Nagarajan, S., Hahn, S., and Lele, S., "Prediction of sound generated by a pitching airfoil: a comparison of RANS and LES," *12th AIAA/CEAS Aeroacoustics Conference (27th AIAA Aeroacoustics Conference)*, Cambridge, Massachusetts, 2006.

[7]Zajamsek, B., Doolan, C. J., Moreau, D. J., Fischer, J., and Prime, Z., "Experimental investigation of trailing edge noise from stationary and rotating airfoils," *The Journal of the Acoustical Society of America*, Vol. 145, No. 4, 2019, pp. 2009–2021.

[8]Zhou, T., Sun, Y., Fattah, R., Zhang, X., and Huang, X., "An experimental study of trailing edge noise from a pitching airfoil," *The Journal of the Acoustical Society of America*, Vol. 145, No. 4, 2019, pp. 2009–2021.

[9]Mayer, Y. D., Zang, B., and Azarpeyvand, M., "Design of a Kevlar-Walled test section with dynamic turntable and aeroacoustic investigation of an oscillating airfoil," *25th AIAA/CEAS Aeroacoustics Conference*, Delft, Netherland, 2019.

[10]Siegel, L., Enfrenfried, K., Wagner, C., Mulleners, K., and Henning, A., "Cross-correlation analysis of synchronized PIV and microphone measurements of an oscillating airfoil," *Journal of Visualisation*, Vol. 21, 2018, pp. 381–395.

[11]Mayer, Y. D., Kamliya Jawahar, H., Szöke, M., Showkat Ali, S. A., and Azarpeyvand, M., "Design and performance of an aeroacoustic wind tunnel facility at the University of Bristol," *Applied Acoustics*, Vol. 155, 2019, pp. 358 – 370.

[12]Devenport, W. J., Burdisso, R. A., Borgoltz, A., Ravetta, P. A., Barone, M. F., Brown, K. A., and Morton, M. A., "The Kevlar-walled anechoic wind tunnel," *Journal of Sound and Vibration*, Vol. 332, No. 17, 2013, pp. 3971–3991.

[13]Mayer, Y. D., Zang, B., and Azarpeyvand, M., "Aeroacoustic investigation of an oscillating airfoil in the pre- and post-stall regime," *Aerospace Science and Technology*, Vol. Accepted/In press, 2020.

[14]McCroskey, W. J., "The phenomenon of dynamic stall." Nasa technical memorandum 81264, Ames Research Center, Moffett Field, California, United States, 1981.

[15]Westphal, W. R. and Godwin, W. R., "Comparison of NACA 65-series compressor-blade pressure distributions and performance in a rotor and in cascade," National advisory committee for aeronautics, United States, 1951.

[16]Corcos, G. M., "Resolution of pressure in turbulence," *Journal of Acoustical Society of America*, Vol. 35.

[17]Bendat, J. S. and Piersol, A. G., *Random data: analysis and measurement procedures*, Vol. 729, John Wiley & Sons, 2011.